Egypt. J. Chem. **Vol. 68**, No. 1 pp. 59 – 68 (2025)

Egyptian Journal of Chemistry

http://ejchem.journals.ekb.eg/

Computational Study of Capturing CO_2 and SO_2 Gases Using Imidazolium-Based Ionic Liquids

Mequanintie Gebeyehu Awoke

Department of chemistry, College of Natural and Computational sciences, Mekdela Amba University, P.O.box:32, Tulu Awulia, Ethiopia

Abstract

The objective of this study was to capture toxic gases like CO_2 and SO_2 using imidazolium-based ionic liquids, 1-butyl 3-methyl-imidazoliumbis(trifluoromethylsulfonyl) imide and 1-ethyl 3-methyl-imidazolium acetate. In this work, DFT method of hybrid correlation functional with B3LYP/6-31++G (d, p) basis set wasused to analyze the mechanism of interaction between toxic gases and ionic liquids based on cations of ionic liquids coupled with an ions of ionic liquids respectively. It has been found that [Bmim][Tf_2N]-SO_2 has greater binding energy than [Bmim][Tf_2N]-CO_2. Therefore, the ionic liquid [Bmim][Tf_2N] seems to be the most suitable option for SO_2 gas capture. Similarly, The ionic liquid [Emim][Ac] has high efficiency to capture the toxic gas SO_2 relative to CO_2. The types of absorption observed in [Bmim][Tf_2N]-SO_2 was Chemisorption while, in [Bmim]Tf_2N]-CO_2 was physisorption. Regarding the intermolecular interaction, the ion pair [Bmim][Tf_2N]-SO_2 was stronger than [Bmim][Tf_2N]-CO_2.Likewise, the ion pairs [Emim][Ac**]**-SO_2 interaction was stronger than [Emim][Ac**]**-CO_2 and the interactions among the molecules in [Emim][Ac**]**-SO_2 was also stronger than that of [Emim][Ac]-CO_2. Hence, [Bmim][Tf_2N] and [Emim][Ac] seems to be the most suitable option to capture SO_2 gas relative to CO_2. The HOMO-LUMO gap for [Bmim][Tf_2N]-SO_2 was the highest showed that highest chemical hardness and the most stable compound.

Keywords: Toxic gas, capture, absorption, DFT, Ionic liquids

1-Introduction

Nowadays, environmental pollution is a global concern. Among these types of pollution, air pollution is attracting increasing attention throughout the world. The combustion of fossil-based fuels results in the emission of a lot of air pollutants to the environment. Sulfur dioxide (SO_2) and carbon dioxide (CO_2) are the main air pollutants causing serious harm to the environment and human health. Mankind is now facing the danger of global warming, which is caused by greenhouse gas emissions, primarily carbon dioxide, along with the risks for the environment on a local scale. [1]. In order to solve such greenhouse gas emission and danger of global warming, computational chemistry uses computer simulation to assist in solving chemical problems. It uses methods of theoretical chemistry incorporated into efficient computer programs to calculate the structures and properties of molecules and solids. Computational chemistry is the application of chemical, mathematical and computing skills to the solution of interesting chemical problems. It uses computers to generate information such as properties of molecules or simulated experimental results. Since computational chemistry has become easier to use, professional computational chemists have shifted their attention towards more difficult modeling problems like capturing of acid gases in liquids or adsorbents [2].

CO_2 is a major greenhouse gas that is responsible for climate change **[3]**. The release of other toxic gases with severe environmental impact is caused by the combustion of fossil fuels, even though CO_2 is the most relevant gas when considering greenhouse effects **[4]**. SO_2 is another harmful gas that is released into the atmosphere and it causes severe problems to the environment including acid rain due to its acidic nature. Hence, controlling acidic gas emissions is frequently considered as a global issue [**5**]. In order to prevent irreversible climate change, it is crucial to reduce the CO_2 emissions and one of the options to achieve this is by the carbon capture and storage (CCS) route [**6**]. The most common capturing technologies for gas capture are based on absorption with aqueous amine solutions, which are also considered as reference methods in comparison with other alternatives which are available method for absorption of acid gases like carbon dioxide in soft drink industries still now. [**7**]. But, amine-based procedures have drawbacks such as amine degradation, equipment corrosion, large energy consumption for solvent regeneration and high operational costs which show the need for new technologies such as those based on ILs **[8]**. Nowadays, ionic liquids (ILs) are under intensive investigation due to their unique properties, such as their negligible vapor pressure, A wide range of temperatures, high thermal and chemical stability, tunable structures,
low melting point, non-flammability, low toxicity, good recyclability, and good solubility for many organic and inorganic materials make them a safer and more environmentally friendly option. Ionic liquids are defined as liquid salts that solely consist of cations and anions, are a solution of a salt in a molecular solvent, and have a melting point of 100 or below.

*Corresponding author e-mail: *mekumekdela21@gmail.com* (Mequanintie Gebeyehu Awoke).
Receive Date: 24 November 2023 Revise Date: 30 December 2023 Accept Date: 01 June 2024
DOI: 10.21608/EJCHEM.2024.250914.8911
©2025 National Information and Documentation Center (NIDOC)

Because the ions are poorly coordinated, this results in these solvents being liquid below 100°C or even at room temperature. [**9**]. Computational methodologies have been extensively used in recent times to complement experimental studies in the ionic liquid area with a great deal of success. When using computational techniques, there are three major conceptual approaches to treating a molecular system. The first is the use of electronic structure methods, which try to capture the most detailed view of a molecular system, short of solving the Schrödinger equation. *Ab initio* and semi-empirical calculations are highly accurate and reliable, as they are derived directly from quantum-mechanical principles; the energy is calculated from a wave function obtained using approximations of varying quality. As a result of this, there is generally a high computational cost associated with these methods, and the simulations are restricted to smaller systems **[10]**.

The DFT approach allows accurate quantification of the strength of IL-acidic gas interactions, intermolecular forces, and molecular and physicochemical changes upon acidic gas capture. The computational requirements for DFT calculations limit the number of molecules, yet the DFT method is still capable of providing a detailed picture of the short-range interactions of IL-acidic gas systems **[11]**. The DFT method is selected because of its low computational cost, good accuracy for structures and thermochemistry, the fact that the density is conceptually simpler than a wave function, and the fact that it uses approximation so that it saves time. The aim of this study was to capture some selected toxic gases in 1-butyl-3-methyl imidazolium bis (trifluoromethyl sulfonyl) imide and 1-ethyl 3-methyl-imidazolium acetate ionic liquid [**12**].

2. Computational Methodology

The ionic liquid and the toxic gases were optimized in the gas phase using the Gaussian 09 Software (Revision D.01) package [**13**]. The DFT method with Becke's Three Parameter Lee Yang& Parr Correlation Functional (B3LYP) and /6-31++G (d, p) basis set was used for the quantum chemical calculations. The lowest lying unoccupied molecular orbitals (LUMO) and the highest occupied molecular orbitals (HOMO) analyses of the molecules were also performed using the DFT (B3LYP) method with a 6-31++G (d, p) basis set. The HOMO-LUMO energy gaps were calculated, which determine the kinetic stability, chemical reactivity, and optical polarizability of CO_2 and SO_2 molecules [**14]**. The toxic gas capture at the molecular level could be related to the strength of the interactions between the ions and the gas molecules. The interaction strength was mainly analyzed based on binding energies (BE). The higher binding energy is adequate for high toxic gas capture efficiency. Binding energy (ΔE) is defined as the energy difference between the energy sum of different complexes and the sum of the energy of each component. A positive binding energy corresponds to favorable binding of the molecules (gases) to the ionic liquids. The binding energy due to the interaction between the IL and the gas molecule is estimated as:

$$BE = E_{IL} - (E_{cat} + E_{ani} + E_{gas}) \ldots\ldots\ldots\ldots\ldots\ldots\ldots (3.1)$$

Where E_{IL}, E_{cat} and E_{ani} Stand for the energies of IL pairs (anion plus cation complex), cations and anions, respectively.

For IL⋯CO_2 and SO_2 complexes, the binding energies were calculated as:

$$\Delta E_{IL_}CO_2 = E_{IL_}CO_2 - (E_{cat} + E_{ani} + E_{CO_2}) \ldots\ldots.. (3.2)$$

$$\Delta E_{IL_}SO_2 = E_{IL_}SO_2 - (E_{cat} + E_{ani} + E_{SO_2}) \ldots\ldots\ldots..(3.3)$$

The absorption energy (E_{abs}) is also estimated using the output values of gases and ionic liquids as:

$$E_{abs}=E(gas\text{-}[Bmim][Tf_2N]) - E([Bmim][Tf_2N]) - (E_{gas} \ldots\ldots (3.4)$$

Where E(gas-[Bmim][Tf_2N]), E[Bmim][Tf_2N] and E_{gas} are the energies of the gas–[Bmim][Tf_2N], [Bmim] [Tf_2N], and the isolated gas, respectively.

Similarly, for the [Emim-Ac], the absorption energy, E_{abs}

$$E_{abs}=E(gas\text{-}[Emim][Ac]) - E([Emim][Ac])(E_{gas})..(3.5)$$

Where E(gas-[Emim][Ac]), E([Emim][Ac]) and E_{gas} are the energies of the gas-[Emim][Ac],[Emim][Ac], and the isolated gas, respectively.

At the molecular level, intermolecular interactions (cation-anion and ion-gas) are the key parameters related to gas capture using ILs [15].

3. Results and Discussions

3.1. Optimized geometries of gases, ionic liquids, and ionic liquid-gas interactions

3.1.1. Minimum energy (optimized) structures of gases

In this work, an investigation of various intermolecular interactions between the gases and the ILs can be undertaken to understand the toxic gases (CO_2 and SO_2) uptake in the two ILs, namely [Bmim][Tf_2N] and [Emim][Ac]. The gases are fully optimized at B3LYP/6-31++G (d, p) using Gaussian 09 software. The analysis of the results was done in a gradual way, starting from the interaction of isolated ions with toxic gas molecules, then evolving to the properties of ion pairs with the gases, and finally studying the behavior of large clusters interacting with CO_2 and SO_2 molecules. The optimized geometries of gases, along with their total energies and gradients, of the two gases used in this study are shown in Table 1. The findings in this table illustrated that the amount of total energy needed for the optimization of gases was tabulated in decreasing order from carbon dioxide to sulfur dioxide gas, and the maximum and minimum total energies for the optimization of these gases were -188.5903926 and -548.599a.u., respectively. It implies that SO_2 has more stable structures than CO_2 **[16]**. The dipole moment for carbon dioxide obtained as a result of the optimization geometry of CO_2 is zero because the two oxygen atoms attract electrons towards themselves from carbon since it has more electro negativity than carbon with the same electro negativity, and finally they become cancelled.

Table 1: **Optimized structure with total energy and RMS Gradient Norm of gases (in a.u)**

Gases	CO_2	SO_2
Optimized structure	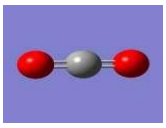	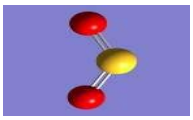
Total energy	-188.5903926	-548.599358
RMS GradientNorm	0.06563623	0.00279980
Dipole Moment(D)	0.0000	1.9984

3.1.2. Minimum energy structures of cations and an ions

In the same way as with the gases**,** the ionic liquids were also fully optimized at B3LYP/6-31++G (d, p) using Gaussian 09 software. During the optimization of cations and anions in ionic liquids, the total energy and RMS gradient norm versus optimization step number plots of a lot of possible structures are obtained. But the structure with the minimum energy was selected for analysis. The atoms with their color codes (grey-carbon, red-oxygen, yellow-sulfur, white-hydrogen, blue-nitrogen, and sky-blue-fluorine) were shown in Figure 1.

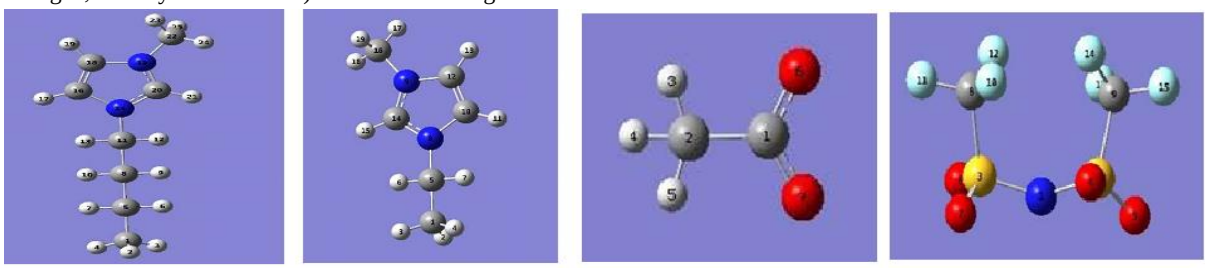

a) $[Bmim]^+$ b) $[Emim]^+$ c) $[Ac]^-$ d) $[Tf_2N]^-$

Figure 1: **Optimized geometries of cations & anions**

The results presented in Table 2 were obtained by optimizing the isolated ions of $[Bmim]^+$ and $[Emim]^+$ at the B3LYP/6-31++G (d, p) level. The bond length of the C-N bond in the imidazolium ring of $[Bmim]^+$ is shorter than the bond length of the C-N bond in the imidazolium ring of $[Emim]^+$. The shorter the distance, the stronger the interaction. Therefore, the interaction among the atoms of $[Bmim]^+$ was stronger than that of $[Emim]^+$. The dihedral angle of some atoms in $[Bmim]^+$ showed less linearity relative to the dihedral angle of some atoms in $[Emim]^+$ because the dihedral angle of atoms in $[Emim]^+$ is exactly 1800, which is linear. The bond length of the C-N bond for both $[Bmim]^+$ and $[Emim]^+$ was in the range of 1.338 Å and 1.470 Å. From the bond angle results, it can be observed that most of the carbon and nitrogen bond angles of $[Bmim]^+$ are smaller than those of carbon and nitrogen in $[Emim]^+$, and this also showed that the bonds are shortened due to the stronger interactions on $[Bmim]^+$ than $[Emim]^+$ **[17]**.

Table 2: **Bond lengths (Å), angles (°) and dihedral Angles (D, deg) of some of the most stable $[Bmim]^+$ and $[Emim]^+$ cations calculated at the B3LYP/6-31++G (d,p) level**

Atoms	**$[Bmim]^+$**	**Atoms**	**$[Emim]^+$**
N14 –C20	1.383	C14– N9	1.467
N15–C22	1.4700	C12–C14	1.345
C16–N14	1.338	N9–C16	1.470
N14–C11	1.470	C10–N8	1.346
C1–C5	1.540	N8–C12	1.467
⟨N15–C18–C20	37.547	⟨C14–C12–N9	38.412
⟨N14–C16–C18	32.546	⟨C10– N8–C12	33.989
⟨C16–C14–N15	35.323	⟨C12–C14–N8	106.858
⟨C20–C18 –N15	106.859	⟨N9–C14–C16	27.145
⟨N14–C16–C20	71.807	⟨N8–C5–C10	25.823
DN14–N15–C20–C22	-179.976	DN9–C10–N8–C5	180.00
DN15–C16–N14–C22	-179.997	DC14–C12–N8–C5	180.00
DC11–N14–C16–C22	179.993	DC16–N9–C10–N8	-180.00
DC22–N15–C20–C18	179.999	DC5–N8–C10–N9	180.00

3.1.3. Minimum energy structures of ionic liquid and cation-an ion interactions

The cation-anion interactions of the ionic liquids in this study were fully optimized at B3LYP/6-31++G (d, p) using Gaussian 09 software. To obtain the most stable structure of 1-ethyl-3-methylimidazolium acetate ([Emim][Ac]), the acetate ion was located at different average positions of 1-ethyl-3-methylimidazolium around the imidazolium ring, and one of the oxygen atoms of the acetate ion was found near the imidazolium ring of H-18 attached to C-17 and another H-25 attached to C-23.

The most stable structure was obtained after the optimization process, which passed 22 optimization steps as shown in Figures 2 and 3. Similarly, 1-butyl 3-methyl-imidazolium bis (trifluoromethylsulfonyl) imide *(*[Bmim][Tf_2N]) ionic liquid was optimized at B3LYP/6-31++G (d, p) level to obtain the most stable (minimum energy) structure. During optimization, it takes a large number of steps (90) relative to [Emim][Ac] by locating the Tf_2N anion at different positions around the 1-butyl 3-methyl-imidazolium ring, and then one of the oxygen atoms, the Tf_2N ion, is near H-21, which is attached to C-20 of the imidazolium ring, which was obtained as the most stable optimized structure of the ionic liquid **[18]**. The most stable optimized structure of [Bmim][Tf_2N] and its total energy and optimization step number plot were shown in Figure 4 and 5.

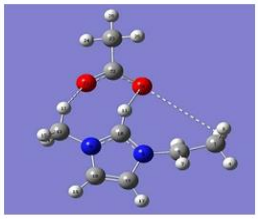

Figure 2: The most stable geometry of [Emim][Ac]

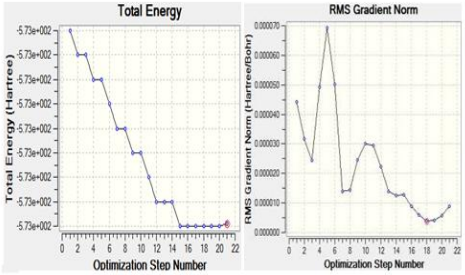

Figure 3: Plots of optimized total energy and RMS Gradient norm of [Emim] [Ac] versus optimization step number

As shown in the first row of Table 3, the C-N bond length in [Bmim][Tf_2N] was longer than the C-N bond length of [Emim][Ac], which illustrated that the cation-anion interaction in [Bmim][Tf2N] was stronger than that of [Emim][Ac] since the longer the distance, the weaker the interactions. The cation-anion distance H19-O32 (1.589Å) of [Bmim][Tf_2N] was shorter than the cation-anion distance H11-O20 (2.226Å) of [Emim][Ac]. Therefore, there were stronger anion-cation interactions in [Bmim][Tf_2N] than [Emim][Ac]. With regard to the bond angles, sulfur has 109.47°in the [Bmim] [Tf_2N] ion pair, which shows tetrahedral types of geometry, and the dihedral angle results illustrate that the presence of both negative and positive angles corresponds to clockwise and anti-clockwise rotations **[17]**. The dihedral angles of [Emim][Ac] show better linearity than those of [Bmim][Tf_2N].

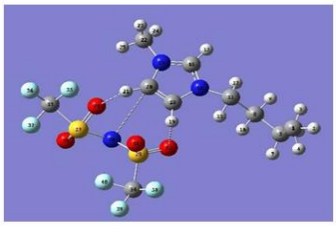

Figure 4: The most stable structure of [Bmim][Tf_2N]

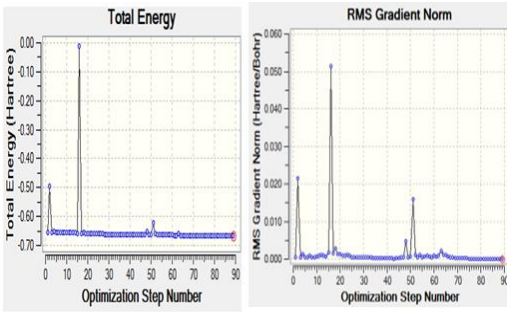

Figure 5: plots of total energy and RMS gradient norm of BmimTf$_2$N versus optimization step number

Table 3: **Bond lengths (Å), angles (°) and dihedral Angles (*D*, deg) of some of the most stable[Bmim][Tf_2N] and [Emim][Ac] ionic liquids calculated at the B3LYP/6-31++G (d,p) level**

Atoms	[Bmim][Tf_2N]	Atoms	[Emim][Ac]
C29–N26	3.547	H13–O21	2.102
H19–O32	1.589	H11–O20	2.226
O29–H21	4.207	C10–N9	1.582
⟨S28–N26–C34	109.471	⟨C22–O22–O20	125.637
⟨S27–O29–C33	82.557	⟨N9–C18–C10	111.060
⟨C33–F35–F36	81.784	⟨C18–C16–N8	106.250
⟨N14–C11–C16	125.768	⟨C10–N9–N8	99.366
D N26–S27–C33–C36	149.832	D C1–C2–O22–C8	151.274
D N26–S27–S28–C34	90.00	D C8–C12–N9–C17	-90.000
D N26–S28–O32–C34	-120.00	D C23–N8–C21–C19	-180.00
D C8–C11–N14–C16	-91.546	D C21–C19–N9–C12	180.00

3.1.4. Minimum energy structures of [Bmim][Tf_2N] -gas interactions

The optimized structure of gases, cations, and anions was optimized together at B3LYP/6-31++G (d, p) using Gaussian 09 software. The gases such as CO_2 and SO_2 were placed in an average position around the 1-butyl-3-methyl imidazolium bis (trifluorosulfonyl methyl) imide ionic liquids, and the optimization was done. Upon optimization, the optimized result provides a lot of possible structures with total energy and root mean square gradient norm versus optimization step number. But the global minimum energy structure was taken into account for further analysis. Figure 6 shows the most stable structures for [Bmim] [Tf_2N]-gas. The [Bmim][Tf_2N]-CO_2 molecule is shown in Figure 6(a), in which CO_2 gas is located around the optimized structure of [Bmim][Tf_2N] on the left side of the Tf_2N ion. The right side is below the average distance of [Bmim][Tf_2N] and above the average distance of [Bmim][Tf_2N], and then, after 120 optimization steps,C-43 of the CO_2 gas near H-24 attached to C-22 of the imidazolium ring is obtained as the minimum energy structure of the ionic liquid-gas interaction. Figure 6 (b) showed the optimized stable structure of [Bmim][Tf_2N]-SO_2, which placed the SO_2 gas around the average position of [Bmim][Tf_2N]. In this case, one of the oxygen atoms of SO_2 is near the H-9 attached to C-8, which is far away from the imidazolium ring **[18]**. The atoms with their color codes (carbon-gray, oxygen-red, nitrogen-blue, hydrogen-white, sulfur-yellow, and fluorine-sky blue) were shown in Figure 6.

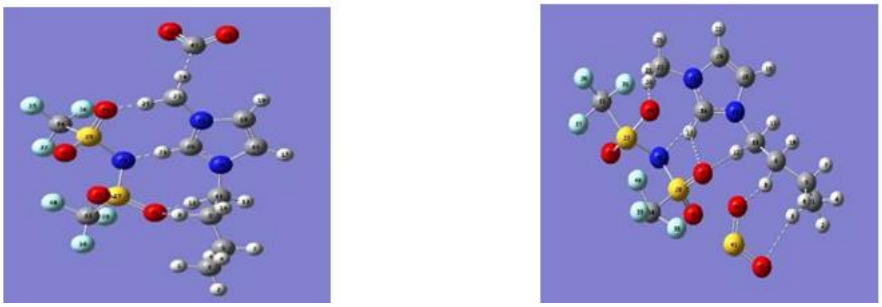

a) [Bmim][Tf_2N]-CO_2 b) [Bmim][Tf_2N]-SO_2

Figure 6: The [Bmim][Tf_2N]-gas optimized minimum energy structures

The optimized geometry parameters such as the bond lengths (Å), angles (°), and dihedral angles (D, deg) for [Bmim][Tf_2N] with SO_2 and CO_2 calculated at the B3LYP/6-31++G (d,p) level of theory are shown in Table 4. The results in this table revealed that the O-H bond length in the ion-pair [Bmim][Tf_2N]-SO_2 was shorter than the ion pair [Bmim][Tf_2N]-CO_2, which implied that the ionic liquid gas interaction was stronger in the ion pair [Bmim][Tf_2N]-SO_2 than the ion pair [Bmim][Tf_2N]-CO_2. The cation-anion distance O29-H25 (1.342Å) of [Bmim][Tf_2N]-CO_2 was shorter than the anion-cation distance O31-H12 (2.676Å) of [Bmim][Tf_2N]-SO2, as shown in the results given in Table 4. This showed that the interaction among the molecules was stronger in the first ion pair than that of the second ion pair. The cation-gas bond length for H24-C43 (1.151Å) in [Bmim][Tf_2N]-CO_2 is shorter than the cation-anion bond length for O31-H9 (1.3671Å), and the cation-gas bond length for O42-H9 (1.663Å) in [Bmim][Tf_2N]-SO_2 was shorter than the cation-anion bond length for O29-H12 (1.873Å). Therefore, the cation-gas interaction was stronger than the cation-anion interaction in both ion pairs **[19]**. The bond angle provided above for sulfur (S28) shows tetrahedral structure in [Bmim][Tf_2N]-SO_2, and the angle of C16 in [Bmim][Tf_2N]-CO_2 also shows tetrahedral geometry. The dihedral angle result reflects the presence of clock-wise and anti-clock-wise rotations in both ion pairs.

Table 4: **Bond lengths (Å), angles (°) and dihedral Angles (D, deg) of the most stable [Bmim][Tf_2N]-CO_2 and [Bmim][Tf_2N]-SO_2 ionic liquids calculated at the B3LYP/6-31++G (d,p) level**

Atoms	[Bmim][Tf_2N]-CO_2	Atoms	[Bmim][Tf_2N]-SO_2
O29–H25	1.342	O31–H12	2.676
H24–C43	1.151	O29–H24	1.873
O31–H9	1.367	O42–H9	1.663
N26–H21	1.939	N26–C16	2.668
⟨C43–O41–O42	127.999	⟨S28–C34–N26	109.471
⟨S27–O29–N26	89.577	⟨S27–C33–O29	42.598
⟨N26–S27–S28	125.963	⟨S41–O42–O43	30.00
⟨C16–N15–N14	109.150	⟨C16–N14–N15	35.323
⟨C20–N15–C18	35.200	⟨N14–C16–C18	37.547
D C33–S27–N26–S28	-159.366	D N26–S27–S28–O31	-90.00
D S27–N26–S28–O32	154.372	D N26–S27–S28–O29	150.00
D O43–C41–O42–C22	172.693	D C8–C11–N14–C16	-91.546
D C22–C16–N15–N14	-156.468	D C11–N14–N15–C20	-180.00

3.1.5. Minimum energy structures of [Emim][Ac]-gas Interactions

The optimized structure of gases, cations, and anions was optimized together at B3LYP/6-31++G (d, p) using Gaussian 09 software. The gases such as CO_2 and SO_2 were placed in an average position around the 1-ethyl-3-methyl imidazolium acetate ionic liquids in order to guess the most stable (lowest energy) structure, and the optimizations were done. Upon optimization, the optimized result provides a lot of possible structures with energy and root mean square gradient norm versus optimization step number. But the global minimum energy structure for [Emim][Ac]-gas was taken into account for further analysis. The optimized minimum energy structure of [Emim][Ac]-CO_2 is given in Figure 7 (a). This structure is obtained as a result of locating the CO_2 gas around the average position of the optimized structure of [Emim][ac]. The CO_2 was near the imidazolium ring and far from the acetate ion. The most stable structure of [Emim][Ac]-SO_2 was given in Figure 7 (b), which was obtained as a result of locating the SO_2 gas around the average position of the optimized structure of [Emim][Ac], and the SO_2 is found near the imidazolium ring while a bit far from the acetate ion [**20**].

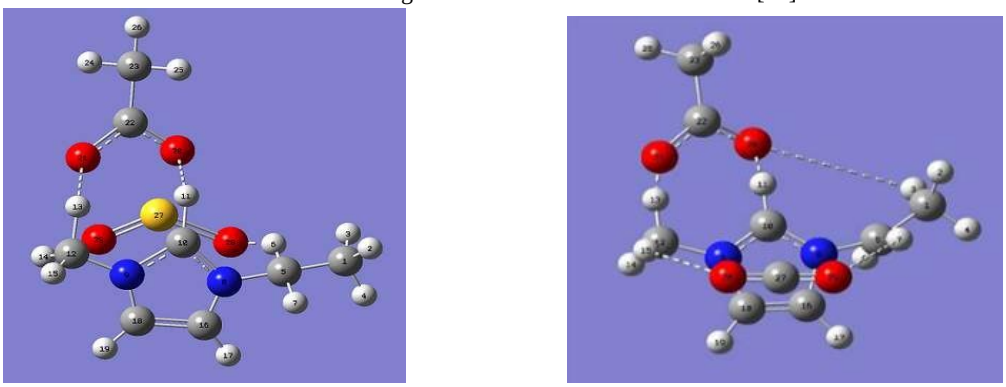

a) [Emim][Ac]-CO_2 **b) [Emim][Ac]-SO_2**

Figure 7: The [Emim][Ac]-gas optimized minimum energy structures

The Bond lengths (Å), angles (°) and dihedral Angles (D, deg) of the most stable structures of [Emim][Ac]-SO_2 and [Emim][Ac]-CO_2 calculated at the B3LYP/6-31++G (d,p) level was shown in Table 5. The results in this table show that the bond length of C-N (1.270Å) in [Emim][Ac]-SO_2 was shorter than the bond length of C-N (1.342Å) in [Emim][Ac]-CO_2. So that the interactions among the molecules in [Emim][Ac]-SO_2 were stronger than those of [Emim][Ac]-CO_2. The cation-gas distances of S27-C10 (1.354Å) in [Emim][Ac]-SO_2 were shorter than the cation-gas distances of C18-O28 (2.839Å) in [Emim][Ac]-CO_2, which implies that the cation-gas interaction is stronger in [Emim][Ac]-SO_2 than in [Emim][Ac]-CO_2. The cation-anion interaction was stronger than cation-gas interactions in [Emim][Ac]-CO_2, whereas the cation-gas interaction of [Emim][Ac]-SO_2 dominates the cation-anion interactions.

Table 5: Bond lengths (Å), angles (°) and dihedral Angles (D, deg) of the most stable [Emim][Ac]-SO_2 and [Emim][Ac]-CO_2 ionic liquids calculated at the B3LYP/6-31++G (d,p) level

Atoms	[Emim][Ac]-SO_2	Atoms	[Emim][Ac] -CO_2
N9-C10	1.332	N9–C10	1.342
N8-C16	1.270	N9–C18	1.388
S27–C10	1.354	C18–O28	2.839
O28–H6	1.046	N9–O28	2.826
H13–O21	2.070	O20-H11	1.443
⟨C22–O20–O21	110.337	O21-H13	1.136
⟨S27–O28–O29	127.992	⟨C27–O28–O29	178.194
⟨N8–C10–C16	116.429	⟨N9–C10–N8	108.573
D O20-C10-C22-N8	169.032	⟨N9–C18–C16	107.172
D N9–C16–C18–C12	179.828	D O28–C27–O29–C5	-110.729
D C10–C5–N8–N9	170.735	D N8–C10–O20–C22	-164.617

3.2. DFT analysis of binding Energy and Absorption Energy for [Bmim][Tf_2N]-gas and [Emim] [Ac]-gas interactions

Gas capture at the molecule level could be related to the strength of the interactions between the ions and the gas molecule. In this work, the interaction strength has been mainly analyzed based on binding energies (BE). The gases, ionic liquids, ionic liquid-gas interaction optimizations, and the binding energy of the interacting molecule were calculated using equation (3.1), and the results were tabulated in Table 6 by calculating the binding energy of the ionic liquid-gas interaction. The results

illustrated that [Bmim][Tf_2N]-SO_2 has greater binding energy compared to [Bmim][Tf_2N]-CO_2. Therefore, the [Bmim][Tf_2N] seems to be the most suitable option for SO_2 gas capture. Since the higher binding energies will be adequate for high toxic gas capture efficiency, The [Bmim][Tf_2N] has high SO_2 gas capture efficiency relative to CO_2. The types of absorption can be differentiated based on the binding energies of IL-gas interactions. Chemical absorption is characterized by the formation of a solute-solvent adduct due to strong localized interaction. The higher the binding energies, the stronger the interactions between the gases and ionic liquids, so that the types of absorption observed in the [Bmim][Tf_2N]-SO_2 interaction were chemisorption, whereas the types of absorption observed in the [Bmim][Tf_2N]-CO_2 interaction were physisorption **[21]**.

Table 6: [**Bmim][Tf_2N]-gas interaction Binding energy(BE)**

Ionic liquid-gas interactions	E_{IL-gas} (eV)	Cations E (Bmim)	Anions E (Tf_2N)	Gas	E_{gas} (eV)	BE (kJ/mol)
[Bmim][Tf_2N]-CO_2	-66372	-11519.9	-49723.3	CO_2	-5131	262.63
[Bmim][Tf_2N]- SO_2	-76169	-11519.9	-49723.3	SO_2	-14928	267.94

Bmim-1-butyl 3-methyl-imidazolium, E_{IL}–Energy of ionic liquids, Tf_2N- bis (trifluoromethylsulfonyl) imide. The absorption energy of [Bmim][Tf_2N]-gas pairs is calculated according to Equation 3.6, as shown in Table 7:
Among the two ion-pairs,[Bmim][Tf_2N]- SO_2 has greater absorption energy which indicates that there was a strong interaction with in the ionic liquid [Bmim][Tf_2N.The higher absorption energy shows that the Chemisorption of SO_2 on to the ionic liquids of [Bmim][Tf_2N] and the lower absorption energy shows the physisorption of CO_2 on to the ionic liquid **[22]**.

Table 7: **Absorption energy of [Bmim][Tf_2N]- gas pairs**

IL-gas	E_{IL-gas} (eV)	$E_{cat-ani}$(eV)	Gas	E_{gas} (eV)	E_{abs} (eV)
[Bmim][Tf_2N]-CO_2	-66371.5	-61240.7	CO_2	-5131.019	0.191
[Bmim][Tf_2N]-SO_2	-76168.7	-61240.713	SO_2	-14928.257	0.246

[Bmim][Tf_2N]-1-butyl 3-methyl-imidazolium bis (trifluoromethylsulfonyl) imide, E_{IL}–Energy of ionic liquids
The binding energy and absorption of the interacting molecule was calculated using equation (3.1) and the results was tabulated in Table 8. The results in this table shows that the correlation between binding energy and the efficiency of ionic liquids to capture the gases that means the higher the binding energy would be adequate to provide high gas absorption affinities **[20]**. The greater binding energy of [Emim][Ac]-SO_2 in the results above shows that the ionic liquid [Emim][Ac] has high efficiency to capture the toxic gas SO_2 and has high affinity for this gas relative to CO_2 The absorption type observed in the [Emim][Ac]-SO_2 was chemical absorption .But the absorption type observed in [Emim][Ac]-CO_2 is physical absorption.

Table 8: **The binding energy of 1-ethyl 3-methyl-imidazolium acetate-gas pairs**

Ionic liquid-gas interactions	E_{IL-gas} (eV)	Cation E (Emim) (eV)	Anion E (Ac) (eV)	Gases	E_{gas} (eV)	BE (kJ/mol)
[Emim][Ac]-CO_2	-20,715.2	-9,373.6	-6,217.6	CO_2	-5131	685.2
[Emim][Ac]-SO_2	-30,506.2	-9,373.6	-6,217.6	SO_2	-14928	1,286.5

[Emim][Ac] -1-ethyl 3-methyl-imidazolium acetate Likewise, the absorption energy of [Emim][Ac]-gas pairs was calculated according to Equation 3.7, as shown in Table 9. The results in Table 9 were obtained by optimizing the ionic liquids and gases at the B3LYP/6-31++G(d,p) level. The higher absorption energy in the ion pair [Emim][Ac]-SO_2 showed that there was a strong interaction between the ionic liquid [Emim][Ac] and SO_2 gas, whereas the lower absorption energy in the ion pair [Emim][Ac]-CO_2 shows that the CO_2 gas was easily desorbed from the ion pair [Emim][Ac]-CO_2.
The high absorption energy indicates the chemisorption of SO_2 onto the [Emim][Ac] ionic liquids, and the low absorption energy in the ion pair [Emim][Ac]-CO_2 revealed the weak physisorption of CO_2 onto the ionic liquid Emim-[Ac] **[22]**.

Table 9: **Absorption energy of 1-ethyl 3-methyl-imidazolium acetate-gas pairs**

IL-gas	E_{IL-gas} (eV)	$E_{cat-ani}$(eV)	Gas	E_{gas} (eV)	E_{abs} (eV)
[Emim][Ac]- CO_2	-20,715.2	15,594.3	CO_2	-5131	10.123
[Emim][Ac]- SO_2	-30,506.2	15,594.3	SO_2	-14928	16.355

[Emim][Ac] -1-ethyl 3-methyl-imidazolium acetate

3.3. Results from molecular orbital analysis

The results obtained by the molecular orbital (MO) analysis are tabulated in Figure 8. The results obtained in this figure show the molecular orbital analysis of cations, ionic liquids, and ionic liquid-gas interactions. The [Bmim]+ is shown in 8 (a), in which the electron density of HOMO was concentrated on the alkyl chain, including the imidazolium ring. But in the case of LUMO, the electron density was concentrated far from the imidazolium ring. Figure 8 (b) showed that in the HOMO-LUMO diagrams of $[Emim]^+$, the electron density in both HOMO and LUMO orbitals is concentrated almost all over the cations of $[Emim]^+$. The HOMO-LUMO diagram of [Emim][Ac] is shown in figure 8 (c), in which there was more electron density concentrated on the HOMO of [Emim][Ac] than the LUMO of this ion pair. Therefore, there was a stronger cation-anion interaction in the case of the HOMO orbitals of the [Emim][Ac] than the LUMO due to the more overlapping of the atomic orbitals of the cations and anions [**23]**. Figure 8 (d) shows the HOMO-LUMO diagram of $[Bmim][Tf_2N]$. Here, the electron density was concentrated on the anions of Tf_2N in the HOMO and on the $[Bmim]^+$ cations in the LUMO. Hence, there was more interaction due to the orbital overlapping of the atomic orbitals of the cations and anions in [Emim][Ac] than in $[Bmim][Tf_2N]$. $[Bmim][Tf_2N]$-CO_2 was shown in Figure 8(e), in which the electron density was fully concentrated on the anions of $[Bmim][Tf_2N]$ in the HOMO orbital diagram and partially concentrated on the cations of $[Bmim][Tf_2N]$ in the LUMO orbital diagram. Therefore, the interaction was slightly stronger in the HOMO than the LUMO. Figure 7 (f) shows the MO diagram of $[Bmim][Tf_2N]$-SO_2, in which the electron density was more concentrated on the anions and some of the cations in the HOMO orbital, and in the case of LUMO, the electron density was more concentrated on either of the ions or on the sulfur dioxide gas. In this case, there was more interaction on the HOMO of the $[Bmim][Tf_2N]$-SO_2 due to more overlapping of atomic orbitals. [Emim][Ac]-CO_2 was shown in Figure 8(g) such that the electron density is more concentrated on the LUMO orbital diagram than that of the HOMO orbital diagram, which results in stronger interaction between the ionic liquids and gases observed in the LUMO orbital diagrams of the [Emim][Ac]-CO_2 due to more overlapping of orbitals **[24]**. Compared to $[Bmim][Tf_2N]$-CO_2, the electron density concentration of [Emim][Ac]-CO_2 was much greater than that of $[Bmim][Tf_2N]$-CO_2. Figure 8 (h) shows the HOMO-LUMO diagram of [Emim][Ac]-SO_2. Here, the electron density was more concentrated on the cations, gas, and some of the anions in the HOMO orbital. In the case of the LUMO orbital, no electron was concentrated on the anion of the ionic liquids. So that there was more IL-gas interaction on the HOMO orbital of [Emim][Ac]-SO_2

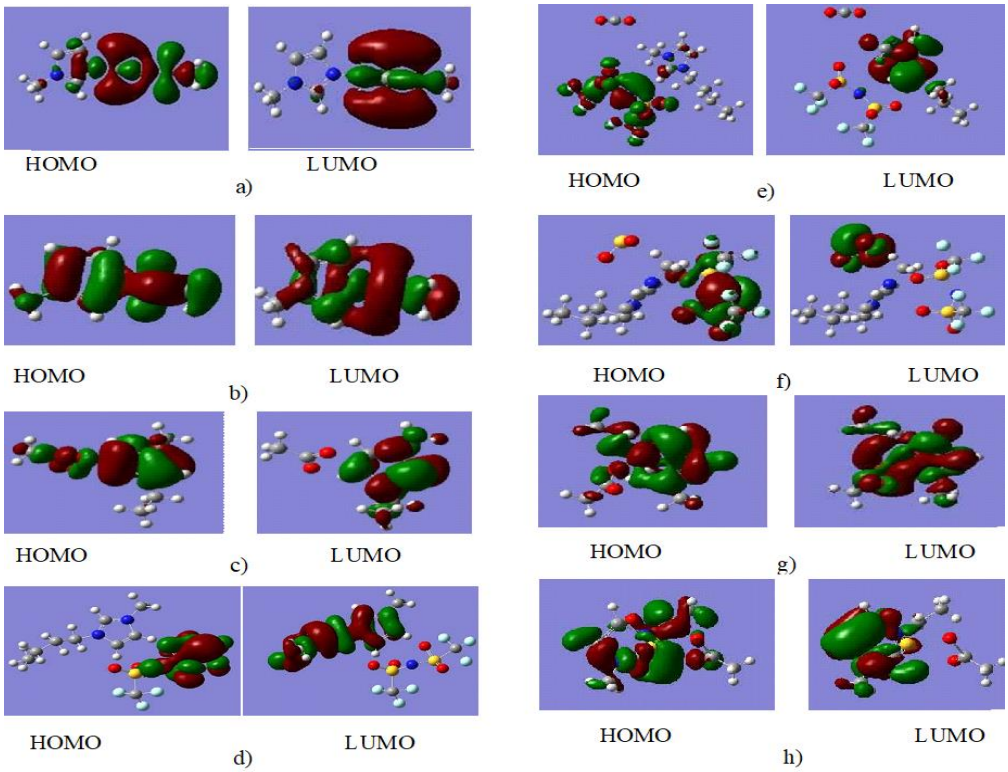

Figure 8: **HOMO-LUMO diagrams of (a) $[Bmim]^+$ (b) $[Emim]^+$ (c) [Emim][Ac] (d) $[Bmim][Tf_2N]$ (e) $[Bmim][Tf_2N]$-CO_2 (f) $[Bmim][Tf_2N]$-SO_2 (g) [Emim][Ac]-CO_2 (h) [Emim][Ac]-SO_2** .

The energy parameters such as HOMO and LUMO energies as well as the global hardness of cation-anion and IL-gas interactions calculated at the B3LYP/6-31++G (d,p) level are summarized in Table 10. The results in Table 10 were attained

by optimizing the ionic liquid-gas interacted molecule at B3LYP/6-31++G (d, p) level. The HOMO-LUMO gap was taken as subtracting HOMO from LUMO. The large HOMO-LUMO energy gaps for [Bmim][Tf_2N]-SO_2 suggest good stability, high chemical hardness, and less reactivity for the [Bmim][Tf_2N]-SO_2 interactions **[22]**. Thus, the chemical hardness of the [Bmim][Tf_2N] was smaller, which indicated that this complex was more unstable than the [Emim][Ac]. A large energy gap implies good thermodynamic stability of the compound, whereas a small energy gap suggests an easy electronic transition. The larger the gap, the higher the stability, and the harder the molecule (complex). Therefore, [Bmim][Tf_2N]-SO_2 had the larger HOMO-LUMO energy gap, the higher stability, and the harder molecule in this result.

Table 10: **Higher Occupied Molecular Orbital (HOMO) and Lower Unoccupied Molecular Orbital (LUMO) energies of cation-an ion and IL-gas interactions**

Cation-Anion & Ioinic liquid-gas interactions	HOMO (a.u)	LUMO Energy (a.u)	HOMO-LUMO gap (eV)	Hardness (a.u)
[Emim][Ac]	-0.3003	-0.1965	2.825	1.41
[Bmim][Tf_2N]	-0.2538	-0.2422	0.316	0.15
[Emim][Ac]-SO_2	-0.2747	-0.2221	1.431	0.72
[Emim][Ac]-CO_2	-0.2273	-0.1867	1.105	0.55
[Bmim][Tf_2N]-SO_2	-0.3601	-0.0821	7.565	3.78
[Bmim][Tf_2N]-CO_2	-0.3110	-0.1349	4.792	2.40

[Emim][Ac]- 1-ethyl 3-methyl-imidazolium acetate [Bmim][Tf_2N]-1-butyl 3-methyl-imidazolium bis (trifluoromethyl sulfonyl) imide

4.Conclusions

A systematic study on the relative ionic liquid-gas interaction energies of imidazolium-based ionic liquids was carried out in this work by the DFT method, B3LYP/6-31++G (d,p). Based on the results obtained from DFT calculations, the following conclusions were drawn: The [Bmim][Tf_2N]-SO_2 has greater binding energy than the [Bmim][Tf_2N]-CO_2. Therefore, the [Bmim][Tf_2N] seems to be the most suitable option for SO_2 gas capture. Since the higher binding energies will be adequate for high toxic gas capture efficiency, the ionic liquid [Bmim][Tf_2N] has high efficiency to capture SO_2 gas. Chemisorption is characterized by higher binding energies, so the types of absorption observed in the [Bmim][Tf_2N]-SO_2 interaction were chemisorption, whereas the types of absorption observed in the [Bmim][Tf_2N]-CO_2 interaction were physisorption. The ion pair [Bmim][Tf_2N]-SO_2 has greater absorption energy, which indicates that there was a strong interaction of SO_2 with the ionic liquid [Bmim][Tf_2N]. The higher absorption energy shows that the chemisorption of SO_2 onto the ionic liquids of [Bmim][Tf_2N]. Physisorption was observed in the ion pairs [Bmim][Tf_2N]-CO_2 and interaction with lower binding energies and absorption energies. The greater binding energy of [Emim][Ac]-SO_2 in the results above shows that the ionic liquid [Emim][Ac] has high efficiency to capture the toxic gas SO_2 and has high affinity for this gas. The absorption type observed in the [Emim][Ac]-SO_2 was chemical absorption since chemical absorption is characterized by higher binding energies. But the absorption type observed in [Emim][Ac]-CO_2 was physical absorption because of the lower binding energies of the ion pairs. The higher absorption energy in the ion pairs [Emim][Ac]-SO_2 shows that there was a strong interaction between the ionic liquid [Emim][Ac] and the gas SO_2. The high absorption energy indicates strong chemisorption of SO_2 onto the [Emim][Ac] ionic liquids, and the low absorption energy in the ion pair [Emim][Ac]-CO_2 showed weak physisorption of CO_2 onto the ionic liquid [Emim][Ac]. Regarding the intermolecular interaction, the ionic liquid gas interaction and the interaction among the molecules were stronger in the ion pair [Bmim][Tf_2N]-SO_2 than the ion pair [Bmim][Tf_2N]-CO_2.

In the same way, the cation-gas interaction was stronger than the cation anion interaction in the ion pairs [Emim][Ac]-SO_2 than [Emim][Ac]-CO_2, and the interactions among the molecules in [Emim][Ac]-SO_2 were also stronger than those of [Emim][Ac]-CO_2. The cation-anion interaction was stronger than the cation-gas interactions in [Emim][Ac]-CO_2, whereas the cation-gas interaction of [Emim][Ac]-SO_2 dominates the cation-anion interactions. The HOMO-LUMO gap for [Bmim][Tf_2N]-SO_2 has the highest energy gap and highest chemical hardness of the rest of the ionic liquid-gas interactions, so that the most stable compound of [Bmim][Tf_2N]-SO_2 from molecular orbital analysis was obtained.

Funding information

This research received no external funding

Author's contribution

The author had done the experiment of the DFT running and calculations. He had also done conceptualization, writing-original draft, formal analysis, communication, review and editing and supervision

Ethical approval

The conducted research is not related to either human or animal use.

Data availability statement

The data set generated during and/or analyzed during the current study are included in the manuscripts.

Declaration of competing interest

The author declares that no conflicts of interest

References

[1] Smith, S.J., van Aardenne, J., Klimont, Z., Andres, R.J., Volke, A. and Delgado Arias, S., 2011. Anthropogenic sulfur dioxide emissions: 1850–2005. *Atmospheric Chemistry and Physics*, *11*(3), pp.1101-1116.

[2] Tadesse, T., 2017. Quantum Mechanical Study on the Effect of Solvent in the Properties of Benzophenone.

[3] De Kleijne, K., Hanssen, S.V., van Dinteren, L., Huijbregts, M.A., van Zelm, R. and de Coninck, H., 2022. Limits to Paris compatibility of CO_2 capture and utilization. *One Earth*, *5*(2), pp.168-185.

[4] Heede, R. (2014). Tracing anthropogenic carbon dioxide and methane emissions to fossil fuel and cement producers, 1854–2010. *Climatic Change*, *122*(1-2), 229-241.

[5] National Greenhouse Gas Inventory Data for the Period 1990–2013, United NationsFramework Convention on Climate Change, Geneva, 2015

[6] Du, Y., Wang, Y. and Rochelle, G.T., 2016. Thermal degradation of novel piperazine- based amine blends for CO_2 capture. *International Journal of Greenhouse Gas Control*, *49*, pp.239-249.

[7] Raynal, L., Bouillon, P.A., Gomez, A. and Broutin, P., 2011. From MEA to demixing solvents and future steps, a roadmap for lowering the cost of post-combustion carbon capture. *Chemical Engineering Journal*, *171*(3), pp.742-752.

[8] Lei, Z., Dai, C. and Chen, B., 2014. Gas solubility in ionic liquids. *Chemical reviews*, *114*(2), pp.1289-1326.

[9] Ramdin, M., de Loos, T.W. and Vlugt, T.J., 2012. State-of-the-art of CO_2 capture with ionic liquids. *Industrial & Engineering Chemistry Research*, *51*(24), pp.8149-8177.

[10] Luo, X.Y., Fan, X., Shi, G.L., Li, H.R. and Wang, C.M., 2016. Decreasing the viscosity in CO_2 capture by amino-functionalized ionic liquids through the formation of intramolecular hydrogen bond. *The Journal of Physical Chemistry B*, *120*(10), pp.2807-2813.

[11] Cao, B., Du, J., Liu, S., Zhu, X., Sun, X., Sun, H., & Fu, H. (2016). Carbon dioxide capture by amino-functionalized ionic liquids: DFT based theoretical analysis substantiated by FT-IR investigation. *RSC Advances*, *6*(13), 10462-10470.

[12] Santiago Aparicio et al. (2011). Study on Hydroxylammonium-Based Ionic Liquids. II. Computational Analysis of CO_2 Absorption. *J. Phys. Chem*, *115*, 12487–12498.

[13] Flick, J., 2022. Simple exchange-correlation energy functionals for strongly coupled light-matter systems based on the fluctuation-dissipation theorem. *Physical Review Letters*, *129*(14), p.143201.

[14] He, Y., Guo, Y., Yan, F., Yu, T., Liu, L., Zhang, X. and Zheng, T., 2021. Density functional theory study of adsorption of ionic liquids on graphene oxide surface. *Chemical Engineering Science*, *245*, p.116946.

[15] García Moreno, G.J., Atilhan, M. and Aparicio Martínez, S., 2015. A density functional theory insight towards the rational design of ionic liquids for SO_2 capture. *PhysicalChemistry Chemical Physics. 2015, V. 17, n. 20, p. 13559—13574.*

[16] Senthil S, Arumozhi S, Madhavan J (2013) Molecular structure and vibration spectra of 2-amino-5-chlorobenzophenone. Department of Physics, Loyola College, India.

[17] Gurau, G., Rodríguez, H., Kelley, S.P., Janiczek, P., Kalb, R.S. and Rogers, R.D., 2011. Demonstration of chemisorption of carbon dioxide in 1, 3-dialkylimidazolium acetate ionic liquids. *Angewandte Chemie International Edition*, *50*(50), pp.12024-12026

[18] García, G., Atilhan, M., & Aparicio, S. (2017). Simultaneous CO_2 and SO_2 capture by using ionic liquids: a theoretical approach. *Physical Chemistry Chemical Physics*, *19*(7), 5411-5422.

[19] Handy, H., Santoso, A., Widodo, A., Palgunadi, J., Soerawidjaja, T.H. and Indarto, A., 2014. H_2S- CO_2 separation using room temperature ionic liquid [BMIM][Br]. *SeparationScience and Technology*, *49*(13), pp.2079-2084.

[20] D'Arminio, N., Ruggiero, V., Pierri, G., Marabotti, A. and Tedesco, C., 2023. Emerging role of carbonyl-carbonyl interactions in the classification of beta turns. *Protein Science*, p.e4868.

[21] Sun, Q., Wang, M., Li, Z., Du, A. and Searles, D.J., 2014. A computational study of carbon dioxide adsorption on solid boron. *Physical Chemistry Chemical Physics*, *16*(25), pp.12695-12702.

[22] Mebi, C.A., 2011. DFT study on structure, electronic properties, and reactivity of cis- isomers of [(NC 5 H 4-S) 2 Fe (CO) 2]. *Journal of Chemical Sciences*, *123*(5), pp.727- 731.

[23] Correa, E., Montaño, D. and Restrepo, A., 2022. Cation··· anion bonding interactions in 1–Ethyl–3–Methylimidazolium based ionic liquids. *Chemical Physics*, *562*, p.111648.

[24] Mohammed, S.A.S., Yahya, W.Z.N., Bustam, M.A. and Kibria, M.G., 2023. Experimental and Computational Evaluation of 1, 2, 4-Triazolium-Based Ionic Liquids for Carbon Dioxide Capture. *Separations*, *10*(3), p.192.